The Effect of Surface Treatments on Thermal Fatigue of H13 Die Steel.

*V.V.Ivanov, ** W.G.Ferguson and *A.F.Trubuhovich

* *Glucina Metals (A Division of Pro Topline Ltd.), New Zealand*
** *The University of Auckland, New Zealand*

(Received April 14, 2003; final form April 24, 2003)

ABSTRACT

Surfaces of die-casting dies are subjected to very severe conditions of cyclical thermal and mechanical load, and chemical and mechanical wear. Dies mostly fail due to a combination of heat checking, erosion, corrosion and soldering.

It is conceivable that appropriate surface treatments and coatings can have a favourable influence on the temperature dependant performance of the surface of the die.

The objective of this study was to examine various surface treatments and coatings, including shot peening, nitriding, nitro-carburising, ion-plasma coatings, electro-spark alloying (deposition) and thermo-reactive diffusion under thermal fatigue conditions.

Thermal cycling tests were conducted by alternate dipping of treated samples in an LM24 alloy melt and then in water. Results and the analyses are presented in this paper. At the end of the test (25000 cycles), thermal fatigue cracks on the substrate were detected only in bare H13 and nitrided specimens.

INTRODUCTION

In service, die-casting dies are subjected to severe mechanical, physical and chemical failure mechanisms, which result in the following forms of die wear: heat checking (thermal fatigue phenomenon) and washout (combined erosion, corrosion and soldering phenomenon) /1/. In fact, these two wearing mechanisms go together, washout weakens the material against heat checking, and heat checking makes the die surface more prone to washout. The temperature of molten aluminium is a critical parameter for both phenomena: the higher the temperature – the higher the stresses and the rate of soldering.

Whilst a number of alternative materials have been tested for aluminium die casting die application, the generic H13 tool steel remains the most popular choice. Unfortunately, for H13 and its heat treatment, there is always the need of compromise between hardness and toughness.

Another possible route to realise desired complex die properties is division of function. A proper coating or treated surface provides protection against wear, and steel is responsible exclusively for load bearing /2, 3/.

PROCEDURE

A thermal fatigue test was conducted with a combined Erosion/Corrosion/Thermal Cycling (ECTC) Test Apparatus, which was designed and built at Glucina Metals to simulate aluminium die casting conditions and be able to test multiple specimens at the same time (Figure 1). A detailed description of the test rig and procedure is given in /1/.

Several alterations were made to the previous test procedure. The first relates to the temperature of the molten aluminium. The melt temperature (T_{melt}) inside the holding furnace, which is about 640°C, has sometimes been regarded as the temperature ($T_{filling}$) at which molten alloy enters the die cavity, and T_{melt} is taken as $T_{soldering}$ to model the growth of soldering

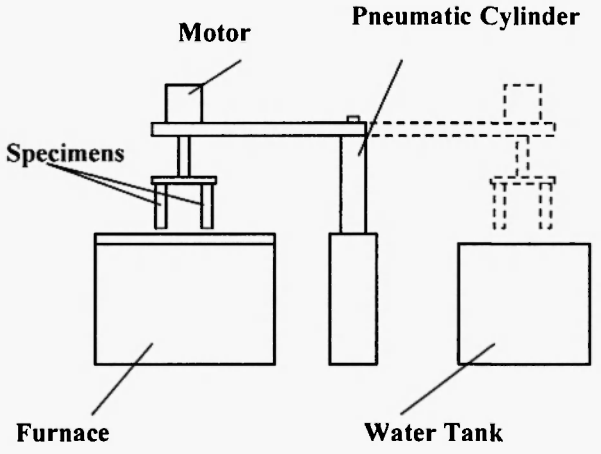

Fig. 1: Schematic diagram of the combined erosion/corrosion/ thermal cycling test rig.

intermetallics during HPDC. Chen *et al.* /4/ indicated that the melt lost its ΔT_s (= T_{melt} – $T_{liquidus}$) before the cast metal entered the die cavity through the gate, particularly during the first stage of filling, when the plunger velocity was low. For this reason, authors concluded that $T_{filling} \sim T_{liquidus}$ = 573°C, or $T_{soldering} \leq T_{liquidus}$ = 573°C (ADC 12 alloy). In order to compromise between the accelerated test and the real temperature profile in a HPDC process, the temperature of the aluminium alloy LM24 was chosen as 650°C compared to 700°C in previous testing /1/.

Six samples were tested at one time, giving a good comparison under identical testing conditions. The base metal was H13 tool steel with the following composition (%): C 0.4, Cr 5.25, Mo 1.5, V 1.0, Si 1.0, Mn 0.35. The specimens were machined and ground by a commercial die manufacturer to a final size of 13 mm-square and 150 mm-length. The grinding pattern was along the length of a specimen. All samples were polished to Ra – 0.4 μm and then given a heat treatment, surface treatment and coatings. The selected treatments are shown in Table 1.

H5 Specimens. This is a bare sample from H13 steel, which was heat-treated using the standard procedure in a fluidised bed.

L-type Specimens. L5 is an Ion Plasma Coating of (Hf,Zr)N, which was produced using an 80%Hf / 20%Zr target in the nitrogen atmosphere. The coating obtained is a very smooth, mirror-like film of yellow-gold colour.

Table 1
Selected surface treatments and coatings

Code	Surface Treatment and Coating
H5	Standard heat treatment
L5	Ion Plasma Coating: (Hf,Zr)N, 450°C.
L6	Electro Spark Deposition (ESD): 1st layer – Co-based superalloy, 2nd layer – TT7K12 (WC, TiC, TaC, Co).
L7	ESD: 1st layer – Mo, 2nd layer – TT7K12.
L8	ESD: 1st layer – Co,Cr,Al,Y master alloy, 2nd layer – TT7K12.
M1	Thermo-Reactive Diffusion (TRD): Fe_2B, 950°C.
M2	TRD: $Cr_{23}C_6$, Cr_7C_3, 1050°C.
N4	Ferritic Nitro-Carburising, 580°C.
N5	Controlled Gas Nitriding, 510°C.
S	Shot Peening: d = 2.3 mm, C = 200%, f = 0.40 - 0.45mm.

All other L-type samples had ESD coatings, which were double-layered. There were several reasons for this. First of all, a double layer can help to overcome the loss of continuity of the coatings, which was noticed in previous testing /1/. Simply put, defects in one layer would be nullified by the subsequent layer, resulting in reduction of the overall defect density. Another advantage of the double layer is being able to use coatings with different thermal and mechanical properties. A typical multilayer coating system generally consists of an interlayer of a compliant material between the substrate and the uppermost layer /5/. During thermal cycling, the single coatings fail due to a mismatch in the coefficient of thermal expansion. Providing a temperature gradient through a multi-layer coating can accommodate the thermal mismatch/thermal fatigue.

M-type Specimens. This type of coating was produced by a Thermo-Reactive Diffusion (TRD) process. Carbide and boride coatings have very good resistance to erosion and corrosion against molten cast metal /6, 7/. TRD coatings are usually carried out at temperatures similar to hardening temperatures for steels; for example 1025-1050°C for H13. Steel substrates are quench-hardened during cooling from the

coating temperatures, followed by tempering. Therefore, distortion may occur. Overcoming distortion is the key point for successful application of the process.

N-type Specimens. These samples represent Ferritic Nitro-Carburising, FNC, (N4) and Gas Controlled Nitriding, NITREG, (N5) surface treatments. The NITREG was applied in a vacuum furnace and the FNC, using a fluidised bed process. FNC is comparable to gas and ion nitriding, but is less brittle and more wear resistant /8/.

S-type Specimens. This sample was shot peened.

One test cycle included: 7 sec. in molten aluminium, 11 sec. in water, and 4 sec. above the molten aluminium. The water bath consisted of tap water and a commercial die lubricant RDL-2588. A lubricant concentration was 1:800, which is about 10 times less than in previous testing. A 5-mm piece was cut off each specimen for examination after 1000, 5000, 10000, 15000, 20000 and 25000 cycles.

All others steps of the experimental procedure were the same as in Part 1 /1/.

RESULTS AND DISCUSSION

In general, the Part 2 testing program went significantly more smoothly than the Part 1 testing. In spite of a considerable reduction in the amount of lubricant (~ 10 times), aluminium stuck to the specimens only a few times (twice - to H5 and once – to N5), compared to dozens of times during the Part 1 testing. As a result, intermetallic compounds were not detected. This confirms how critical the melt temperature is for soldering formation /9/, if reduction of melt temperature from 700°C (Part 1) to 650°C (Part 2) gave such different behaviour.

As expected, an overall crack pattern is not as obvious as it was in the Part 1 testing. Moreover, the longitudinal cracks, developed in the N-type specimens during the Part 1 test /3/, were not detected. Decreasing the temperature gradient on the specimen's surface mitigates thermal stresses, which extends the thermal fatigue life of steel. When the temperature difference ΔT for the thermal cycles is less then the critical temperature difference ΔT_0 of the thermal fatigue crack initial (TFCI) life, the TFCI life of hot-work die steel tends to infinity /10/. The along-the-length grinding pattern and very fine polishing (Ra < 0.4 μm) of specimens also contribute to this phenomenon.

H5 Specimens. The microstructure of the H5 specimen after 25000 cycles is shown in Figure 2.

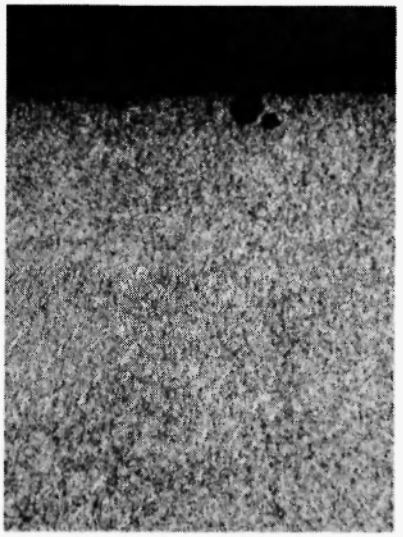

Fig. 2: Microstructure of the H5 specimen, 5000 cycles, 2.5% nital, 200×.

Initial microstructure represents a typical tempered martensite. The pit-like defects (dark spots on and beneath the surface) are still present in the material, only their size is less than twenty microns compared to hundreds of microns in the first test programme/1/. The size of surface defects for the given conditions becomes a matter of stress severity, i.e. the bigger the thermal shock the bigger the surface defects. Since the melt temperature in the Part 2 test programme is lower by 50°C compared to that in the Part 1, the size of the surface defects is also smaller.

The EDX and XRD analyses have shown that the grey substance in pits consists of complex spinel-type oxides. The presence of soldered casting alloy or intermetallic compounds, as mentioned earlier, was not found.

The transverse crack pattern of the H5 specimen after 25000 cycles is shown in Figure 3.

All cracks are very narrow and superficial. The crack parameters of the H5 specimen after 25000 cycles

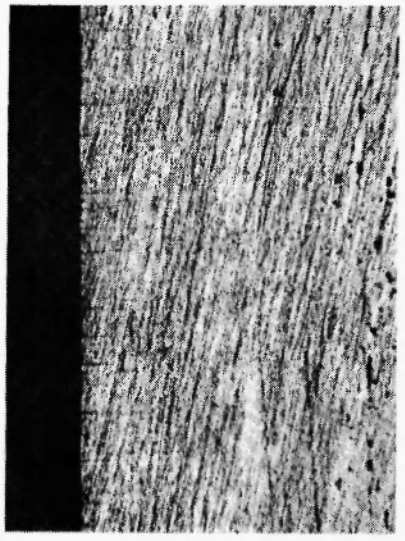

Fig. 3: Transverse crack pattern of the H5 specimen, 25000

are given in Table 2.

Table 2
Crack parameters of the tested specimens after 25000 cycles.

Code	Transversal Cracks			
	l_{max}, μm	Σl, μm	l_a, μm	n, cr./mm
H5	200	5150	128	4
N5	130	1850	123	1.5

The surface hardness values of the H5 specimen gradually reduce from (470 – 480) H_v at the beginning to (400 – 420) H_v at the end of the test (Figure 4).

Compared to the H4 specimen /1/, the retained hardness of the H5 sample is higher than that of the H4 {(290 – 305) H_v} for both surface and bulk areas. Also, the H4 specimen has lost its initial hardness during the first 1500 cycles, whereas H5 hardness gradually reduces throughout the test. The higher hardness (yield strength) means that material has better resistance to thermal fatigue and indentations.

N4 and N5 Specimens. The initial microstructure of the N4 and N5 samples is similar, featuring a distinctive nitride and carbo-nitride diffusion zone of 50 - 80 μm in depth. During the thermo-cycling, transformations in microstructure were not observed in either specimen.

The changes of the case micro-hardness during the thermo-cycling are shown in Figure 4. The micro-hardness of the N4 specimen gradually drops from 930 H_v (initial) to 800 H_v at 25000 cycles. The N5 sample has higher initial micro-hardness (1200 H_v), but it decreases rapidly during the first 1000 cycles (970 H_v) and then slowly reaches 800 H_v at 25000 cycles. Probably because carbo-nitride phases are less inclined to coagulation during the heating than nitrides, the N4 specimen shows better tempering resistance than N5.

Figure 5 displays the regular transversal cracks, which originate in oxide layer (grey). Eventually, some of them can initiate cracks in the die metal when the tensile stress exceeds the elastic limit.

However, there were no transversal cracks observed on the surface of metal in the N4 specimen. Nevertheless, a few narrow, hardly visible cracks were found on the surface of the N5 sample (Figure 6). It is reasonable to assume that nitride phases are responsible for this. Generally, nitride compounds are more brittle than carbo-nitrides and, consequently, they have less ability to accumulate plastic deformation before fracture occurs.

The measured crack parameters of the H5 and N5 specimens are presented in Table 2. The N5 specimen has a crack density (n) and the cumulative crack length (Σl) more than two times smaller than the H5 sample.

S Specimens. The microstructure of the S specimen represents the martensitic structure with a wave-like peened surface. The difference between the initial state and that after thermal cycling is the presence of an even oxide layer, which duplicates the surface relief. The dents from the shots in the steel matrix feature on the surface of the sample. There were no transversal cracks found on the surface of the S-specimen.

The initial subsurface micro-hardness of the S-sample, and that following a certain amount of thermo-cycling is shown in Figure 4. At the first stage of cycling (1000 cycles), the hardness of the S-specimen dropped faster (from 540 to 490 H_v) than that of H5 (from 490 to 470 H_v), but then it maintains the positive difference of 10-20 units up to the 25000 cycles.

L5 Specimens. Thickness of the Hf/Zr nitride film is about 2 μm and measured surface micro-hardness is 950

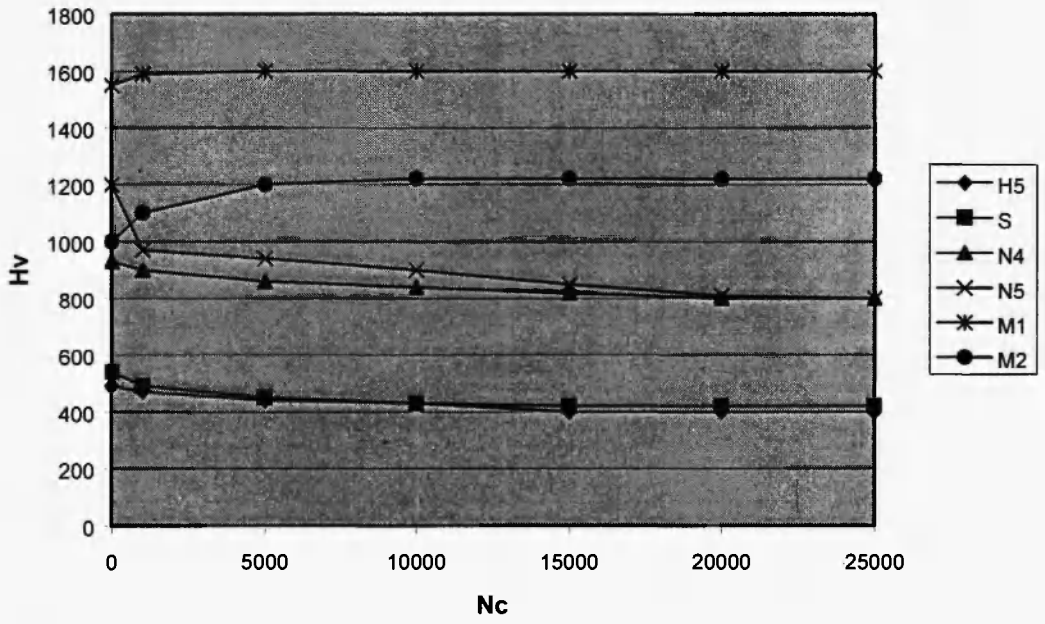

Fig. 4: Case microhardness values (H_V) versus number of cycles (N_C) of the tested specimens.

Fig. 5: Edge of the N4 specimen, 25000 cycles, 50×; unfinished grinding process; remains of oxides (grey) with transversal cracks, which do not propagate into steel (white).

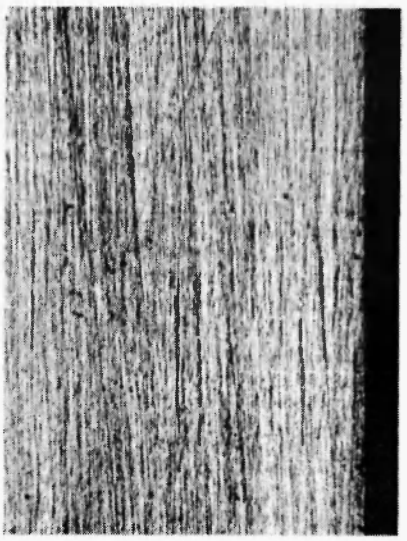

Fig. 6: Transverse crack pattern of the N5 specimen, 25000 cycles, 50×; fine transversal

H_V. In general, the coating performed well during testing, but in some spots it lost integrity and very small pits (up to 5 μm) originated on the surface.

Transversal cracks were found neither on the coating nor on the substrate of the L5 specimen after 25000 cycles.

L6 – L8 Specimens. These samples exhibit a double-layered ESD coating. The outer layer, which is the same for all three specimens, represents a hard alloy TT7K12 (81% WC; 4% TiC; 3% TaC and 12% Co). The inner layer is different for each sample: Co-base super alloy – for L6; Mo – for L7; and Co/Cr/Al/Y-master alloy (23% Cr; 12% Al; 0.5% Y; Co – rem.) – for L8.

The initial microstructure of all ESD specimens is quite similar: very well metallurgically bonded to the substrate without a distinct interface between the two layers and with considerable roughness on the surface (Figure 7). The coating is not perfect as fine porosity is present. The number of pores increases with thermo-cycling (Figure 8). Also, longitudinal and transversal cracks initiate in the coating. It appears the cracks originated on defects (pores) and propagated towards the surface through the more brittle layer. The pores are generated on the interface between the two layers. None of the cracks goes through the inner layer and substrate beneath the coating retains its continuity and integrity. The thickness of the coating varies from 10 to 20 μm. The micro-hardness of the outer layer varied from 1280 to 1400 H_v and did not change during the test.

Transversal cracks were not found on the substrate of any ESD specimens.

M1 and M2 Specimens. The M1 specimen was treated by a TRD process to produce an Fe_2B phase on the surface. The initial microstructure of the sample (Figure 9) reveals a layer of columnar iron boride with about 70 μm thickness and about a 100 μm diffusion zone. After the first 1000 cycles, transversal cracks appear along the columnar grains and further cracks parallel to the surface appear in the film (Figure 10). Eventually, the coating breaks off exposing the steel surface to lubricant and molten metal.

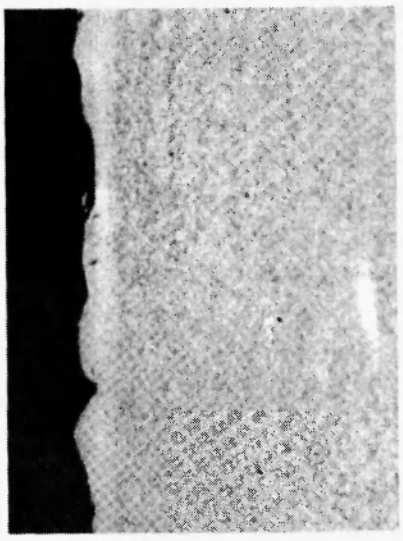

Fig. 7: Initial microstructure of the L8 specimen, 2.5% nital, 200×.

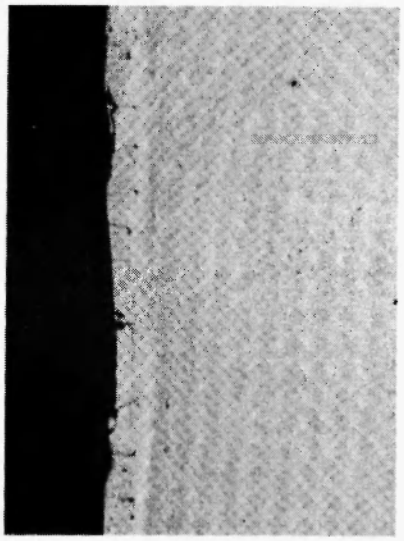

Fig. 8: Microstructure of the L8 specimen after 25000 cycles, 2.5% nital, 200×.

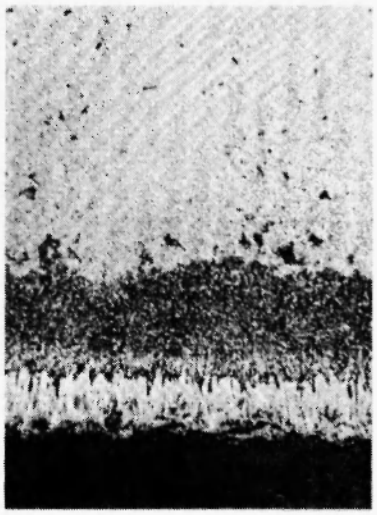

Fig. 9: Initial microstructure of the M1 specimen, 2.5% nital, 200×.

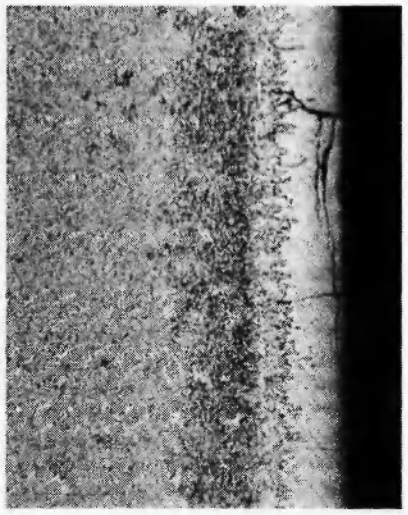

Fig. 10: Microstructure of the M1 specimen after 1000 cycles, 2,5% nital, 200×.

There is a very soft (~250 H_v) intermediate phase (light grey) between the boride and the substrate, where the transversal cracks were initiated. The micro-hardness of this soft matrix did not change during the test. It is widely postulated that a coating scheme, which provides a way to create a compliant interface to accommodate a mismatch stress, will improve the thermal fatigue resistance of dies /5/. Nevertheless, this compliant interlayer should not be softer and weaker than the substrate and should have sufficient yield strength and toughness to cope with thermal stresses.

The initial micro-hardness of the M1 coating was about 1550 H_v, then slightly increased during the first stages of cycling (up to 1600 H_v) and maintained this level up to the end of the test (Figure 4).

The M2 specimen was treated by the TRD process to produce chromium carbides like $Cr_{23}C_6$ and Cr_7C_3. The initial microstructure of the sample (Figure 11) shows a compact layer of chromium carbides with good adhesion to the substrate. Nevertheless, a certain number of fine pores are present. After the first stages of thermo-cycling, some transformations have occurred at the coating/substrate interface, which lead to the appearance of small internal cracks and an increase in the amount of volumetric defects (porosity) in the coating. Subsequently, these led to coating deterioration and formation of pit-like defects (Figure 12), which had been discussed in Part 1 /1/.

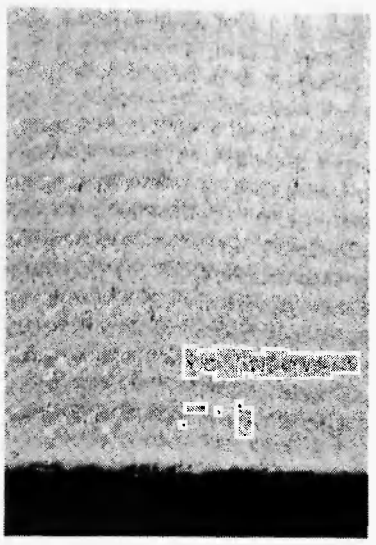

Fig. 11: Initial microstructure of the M2 specimen, 2.5% nital, 200×.

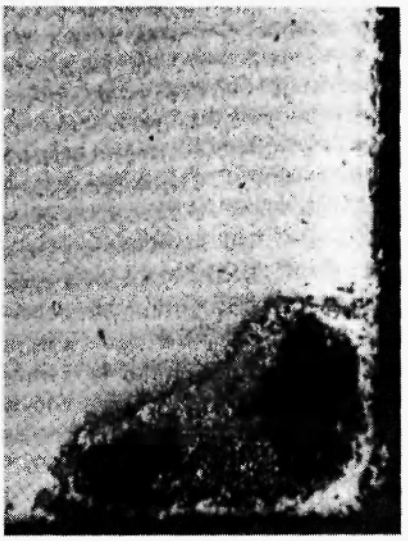

Fig. 12: Microstructure of the M2 specimen after 25000 cycles, 2.5% nital, 200×.

The pattern of the coating's micro-hardness change is pretty much similar to that for M1; only the level of values is lower – from 1000 to 1220 H_v (Figure 4). The hardness of the interfacial layer, adjacent to the chromium carbide coating, was between 450 – 700 H_v and was retained at this level up to the end of the test. Such a transition between the substrate and the coating seems to be much more suitable than that in the M1 specimen.

Fig. 13: M1 specimen after 25000 cycles, 50×.

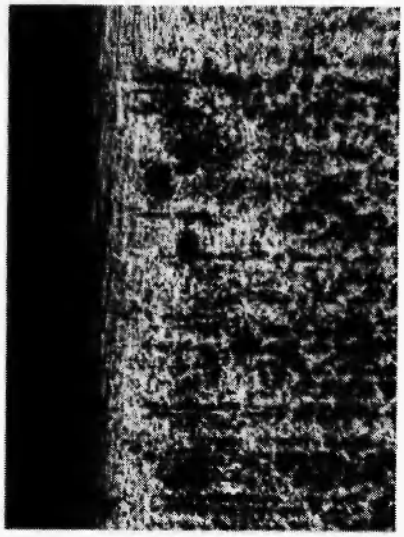

Fig. 14: M2 specimen after 25000 cycles, 50×.

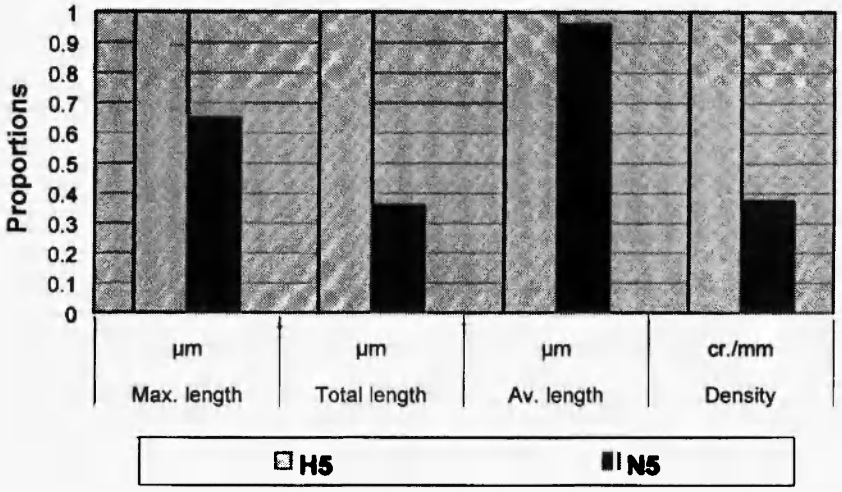

Fig. 15: Cumulative relative crack parameters of the H5 and N5 specimens.

The surface condition of the M1 and M2 coatings after 25000 cycles are displayed in Figures 13 and 14. The M1 coating has transversal cracks, pits of various size and areas detached from the substrate. The M2 coating shows pits, which are beginning to combine in transversal lines, no cracks and no significant damages. However, no substrate cracks were found in either the M1 or M2 specimens.

The only specimens that have thermal fatigue cracks present on the substrate during this test programme, were H5 and N5. Relative crack parameters for these two samples are given in Figure 15. The N5 specimen has a crack density and total crack length about three times less than that for H5 sample.

Thus, the study has shown that various surface treatments and coatings can improve thermal fatigue and washout resistance of die materials. If the die surface requires a very low roughness ($R_a \sim 1\mu m$), the die manufacturer may choose between FNC and IPC. If the requirements of die surface roughness are not strict – the choice may be between shot peening, ESD or TRD. Moreover, the proper coatings and surface

treatments allow reducing significantly (or even eliminating) the use of lubricant, which has important environmental and commercial aspects.

CONCLUSIONS

1. Reducing the melt temperature from 700°C to 650°C mitigates the difference between the HPDC conditions and the thermal fatigue test, and makes assessing the tool steel performance more realistic. However, to achieve substantial crack formation, it is necessary to increase the number of thermo-cycles.
2. The concentration of the lubricant release agent RDL-2855 was reduced approximately by 10 times compared to the Part 1 test. This resulted in a significant reduction of the amount of lubricant residue build-up on the specimens during cycling.
3. Soldered casting alloy and intermetallic compounds were not found in the tested specimens, in spite of a reduction in die lubricant consumption. This underlines the importance of temperature as a critical factor in the soldering process.
4. The nitro-carburised specimen (N4) shows better tempering resistance than the nitrided sample (N5), probably because carbo-nitride phases are less inclined than nitrides to coagulation during the heating.
5. The ion-plasma coating (L5) has shown a slight surface deterioration (less than 5 μm), presumably by reason of its thinness (~2 μm). For possible future implementation into dies manufacturing, the process parameters should be worked out for obtaining a thicker coating (at least about 3-5 μm).
6. In general, the ESD specimens (L6 – L8) displayed an excellent metallurgical bond between the substrate and the inner coating layer. However, the outer coating layer contained some cracks and pores, but retained its adhesion to the inner coating. The search for the best substrate/coating combination should be continued.
7. The chromium carbide TRD coating (M2) resisted thermal fatigue without cracking and better than the iron boride (M1) coating, although it showed some surface deterioration (pits).
8. Only two of the tested specimens (H5 and N5) have demonstrated thermal fatigue cracks in the substrate, and N5 sample has shown a crack density and total crack length about three times less than the H5.

REFERENCES

1. V.V. Ivanov, I.R. Paine and P.J. Revnyuk, *High Temp. Mater. Processes (London)*, **21**, (1-2), 65-78 (2002).
2. S. Gopal, A. Lakare and R. Shivpuri, *Surf. Eng.*, **15** (4) 297-300 (1999).
3. S. Wang, Y. Li, M. Yao and R. Wang, *J. Mater. Process. Technol.*, 73, 64-73 (1998).
4. Z.W. Chen, M.Z. Jahedi and J.A. Law, *Transactions, NADCA 20th International Die Casting Congress*, T99-085 (1999).
5. D.G. Bhat, V. Gorokhovsky, R. Shivpuri and K. Kulkarni, *Transactions, NADCA 20th International Die Casting Congress*, T99-112 (1999).
6. A. Agarwal and N.B. Dahotre, *Mater. Charact.*, 42, 31-34 (1999).
7. S. Harper and T. Arai, *Die Casting Engineer*, 84-94 (Mar.-Apr. 2000).
8. L. Epler and L. Rickman, *Die Casting Engineer*, 70-73 (Mar.-Apr. 2000).
9. S. Gopal, A. Lakare, K. Kulkarni and R. Shivpuri, *Transactions, ADCA Die Casting 2000 Conference*, Australia, 34/1 (2000).
10. L. Guobin, L. Xiangzhi and J. Wuc, *J. Mater. Process. Technol.*, 74, 23-26 (1998).